Case Studies in Thermal Engineering 28 (2021) 101575

Contents lists available at ScienceDirect

Case Studies in Thermal Engineering

journal homepage: www.elsevier.com/locate/csite

Multispectral infrared absorption spectroscopy for quantitative temperature measurements in axisymmetric laminar premixed sooting flames

Liuhao Ma [a,b,*], Kun Duan [b], Kin-Pang Cheong [c,**], Chaokai Yuan [d], Wei Ren [b]

[a] Laboratory for Advanced Combustion, School of Automotive Engineering, Wuhan University of Technology, Wuhan, Hubei, China
[b] Department of Mechanical and Automation Engineering, and Shenzhen Research Institute, The Chinese University of Hong Kong, New Territories, Hong Kong, SAR, China
[c] School of Aeronautics and Astronautics, Sichuan University, Chengdu, Sichuan, China
[d] State Key Laboratory of High Temperature Gas Dynamics, Institute of Mechanics, Chinese Academy of Sciences, Beijing, China

ARTICLE INFO

Keywords:
Temperature measurement
Sooting flame
Multispectral infrared absorption spectroscopy
Optical sensing

ABSTRACT

Multispectral infrared absorption spectroscopy was developed for *in situ*, non-intrusive and quantitative measurements of temperature distributions in laminar premixed ethylene/air sooting flames. Tunable distributed feedback (DFB) lasers near 1343 nm, 1392 nm and 2482 nm were used to exploit multiple H_2O absorption lines with varied temperature sensitivities. Scanned-wavelength direct absorption spectroscopy combined with the multi-line profile-fitting strategy was conducted for temperature sensing along the line-of-sight. This optical method was first numerically investigated for representative combustion fields to evaluate the measurement accuracy and uncertainty under different noise levels (2–10%). In the experiment, optical measurements were performed at different heights above the burner (3–15 mm) under three representative flame conditions (equivalence ratio Φ = 1.9, 2.1 and 2.3) with different co-flow gases (N_2 and air). Our measurements successfully captured the temperature field and were in excellent agreement with the thermocouple data within the high-temperature region. A slight temperature rise in the central flame was quantitatively differentiated when co-flow gas was changed from N_2 to air. The proposed method proves to be a promising combustion diagnostic technique for quantitative temperature measurements with the line-of-sight information.

1. Introduction

Laminar premixed sooting flames have been extensively used for studying soot formation and novel diagnostic techniques due to the good temporal stability and spatial uniformity [1–3]. The quasi-steady and quasi-uniform flame is also suitable for the verification and validation of chemical kinetic mechanisms and soot models [4–6]. In these studies, the thermochemical profiles were normally investigated along the axial direction perpendicular to the burner surface by assuming the flame to be one-dimensional (1D). As a consequence, very limited information of two-dimensional (2D) thermochemical distributions was reported for such burner-stabilized

* Corresponding author. Laboratory for Advanced Combustion, School of Automotive Engineering, Wuhan University of Technology, Wuhan, Hubei, China.
** Corresponding author.
E-mail addresses: liuhaoma@whut.edu.cn (L. Ma), kpcheong@scu.edu.cn (K.-P. Cheong).

https://doi.org/10.1016/j.csite.2021.101575
Received 18 July 2021; Received in revised form 5 October 2021; Accepted 20 October 2021
Available online 22 October 2021

flames. For instance, in the well-structured database from International Sooting Flame (ISF) workshop [7], thermochemical parameters were generally provided in 1D format. However, recent experimental measurements and computational fluid dynamics (CFD) simulations have revealed that such flames are not strictly 1D [8–10]. The evident 2D effects induced by the buoyancy-driven hot downstream and the enhanced heat transfer to the cool co-flow stream may cause non-negligible errors in kinetic modeling [11]. As the soot formation has evident temperature dependence, the flame temperature has been identified as the most significant parameter in sooting flame studies [12–14]. With a more strict constraint on the 2D temperature profile, the simulated soot distribution was found to be more consistent with experimental data [15].

Thermocouple has been frequently used for flame temperature measurements. The spatially-resolved temperature profile can be obtained by the pointwise measurement, but thermocouple has limited use due to its intrusive perturbation of the local combustion field and the essential requirement of the heat-transfer correction to raw data. Additionally, the hostile environment with soot deposition and catalytic effect further introduces measurement uncertainties [16]. In comparison, the optical technique has become more attractive for flame diagnostics favoured for the non-intrusive nature and spatially-resolved capability.

Camera- and laser-based diagnostic techniques are the two major optical methods used for studying sooting flames. The camera-based technique utilizes the collected multi-directional and multi-spectral soot radiation to reconstruct the temperature field. This method has been successfully used for temperature measurement in lab-scale sooting flames [17,18]. However, frequent camera pre-calibrations, specially designed mathematical models and sophisticated algorithms are typically required to ensure reliable and accurate measurements. In terms of laser-based measurements, laser-induced fluorescence (LIF) and coherent anti-Stokes Raman scattering (CARS) are the common approaches for spatially-resolved thermometry [19,20]. The two methods usually require expensive and cumbersome high-power laser sources (e.g., Nd:YAG and dye lasers) [21]. Additionally, calibration is also required to realize quantitative measurement.

Laser absorption spectroscopy (LAS) can provide highly quantitative and calibration-free measurements using compact, robust and simple diagnostic systems [22–24]. Although the line-of-sight (LOS) integration nature partially limits the measurement in non-uniform environments, two-dimensional measurements can be achieved using improved strategies, including tomographic reconstruction and multiline absorption thermometry [25,26]. The two strategies have been well-validated and widely used for quantitative measurements in flames [27–33]. However, the conventional tomographic reconstruction requires frequent mechanical translation to collect the absorption signals from multiple positions and directions, which limits the spatial resolution. Although advanced optical configuration with multiple photodetectors or CCD camera overcomes such issues [34,35], the consequent cost and complexity increase a lot. In addition, the tomographic reconstruction suffers moderate in measuring the low-temperature region due to the weak absorption near the flame boundary region. In comparison, multiline thermometry can be used to resolve LOS temperature distributions from high-temperature region to cool flame edge. This method utilizes the multiple spectrally-resolved absorption features from a single LOS measurement to reconstruct the non-uniform distribution, making it attractive in axisymmetric flame measurements [32]. Therefore, we selected the multiline thermometry to perform the measurements of sooting flames in the current work. Note that, the target laminar premixed sooting flame stabilized on McKenna burner is the benchmark flame collected in International Sooting Flame (ISF) workshop. Such flame is axisymmetric and steady. However, the radial distribution of temperature in this flame is not well measured due to its sooting environment for both contact and non-contact methods. LAS is a promising method for sooting flame due to its calibration-free and harsh-environment endurable features. To the best of the authors' knowledge, attempt in applications of the multispectral absorption-based thermometry in this flame has not been reported elsewhere. Our main scope of this work is to optimize the selection of multiple absorption lines for temperature measurement in the target flame and develop strategy to resolve the temperature distribution along the line-of-sight optical path (i.e., the radial distribution).

In this work, we present the development of multispectral infrared absorption strategy for temperature measurement in premixed sooting flames. A mid-infrared distributed feedback (DFB) laser near 2.5 μm and two near-infrared diode lasers near 1.4 μm were employed to target multiple H_2O absorption lines. Regarding the measurement accuracy and uncertainty, the performance of the proposed method was first numerically evaluated under typical sooting flame conditions with different noise levels (2–10%). Experiments were performed at different equivalence ratios ($\Phi = 1.9$, 2.1 and 2.3) and co-flow gases (N_2 and air). The slight temperature increase within the central flame due to the local re-burn near the flame edge was successfully captured. The current method proves not only show the capability of quantitative measurements but also the ability to differentiate the temperature nuance when boundary condition varies.

2. Measurement principle

The fundamental principles of LAS have been well detailed in the previous literature [36]. Here we only reproduce a brief description of spectroscopic fundamentals relevant to the current measurements to clarify the basic definition and nomenclature, and inform the reader how the gas temperature is inferred from the measured attenuation of laser intensity. When a collimated, spectrally-narrow laser beam at a specific optical frequency ν (cm^{-1}) passes through a non-uniform absorbing gas medium with an accumulated optical absorption length L (cm^{-1}), the fractional transmission of the laser intensity is governed by the well-known Beer-Lambert law:

$$\left(\frac{I_t}{I_o}\right)_v = \exp(-\alpha_v) = \exp\left(-\int_0^L S_i(T(r))P(r)X_{abs}(r)\varphi_v dr\right) \tag{1}$$

Where I_0 and I_t represents the incident and transmitted laser intensities, respectively, α_v indicates the spectral absorbance at optical

frequency ν [cm^{-1}], $S_i(T(r))$ [cm^{-2}·atm^{-1}] is the temperature-dependent line-strength of the particular ro-vibrational transition i at local gas temperature $T(r)$, $P(r)$ [atm] is the total gas pressure, $X_{abs}(r)$ is the local gas concentration of the absorbing species, r is the certain position along the line-of-sight (LOS), and φ_ν [cm] is the line-shape function. As φ_ν is normalized to 1, the integrated absorbance (A_i) across the entire absorption feature is expressed as:

$$A_i = \int_0^L S_i(T(r))P(r)X_{abs}(r)dr \tag{2}$$

For the flame environment with uniform pressure, Equation (2) is simplified to

$$A_i = P\int_0^L S_i(T(r))X_{abs}(r)dr \tag{3}$$

As the information of the non-uniform thermochemical distribution is embedded in Equation (3), measurements of the multiple absorption features are required to infer the unknown variables in temperature ($T(r)$) and gas concentration ($X(r)$) profile functions. When a series of absorption transitions with different temperature-dependence are selected, a non-linear equation set can be generalized as:

$$\begin{cases} A_1 = P\int_0^L X_{abs}(r)S_1(T(r))dr \\ A_i = P\int_0^L X_{abs}(r)S_i(T(r))dr \\ \quad\vdots \\ A_m = P\int_0^L X_{abs}(r)S_m(T(r))dr \end{cases} \tag{4}$$

When the number of total equations is larger than or equal to the number of unknown variables, the equation set can be readily solved by the non-linear least-square fitting:

$$\min_{T(r),X_{abs}(r)} \sum_{i=1}^{m} \left(\frac{P\int_0^L X_{abs}(r)S_i(T(r))dr - A^i_{measured}}{A^i_{measured}} \right)^2 \tag{5}$$

The Levenberg-Marquardt algorithm was used for global convergence during the fitting process. In addition, the thermochemical distributions of the sooting flame under different co-flow conditions can be described by the following profile function:

$$f(r) = \begin{cases} \beta_2 + \dfrac{\beta_1 - \beta_2}{1 + e^{(r-\beta_3)/\beta_4}} & \text{N}_2\text{\_Coflow} \\ \dfrac{\beta_1'}{1 + e^{(r-\beta_2')/\beta_3}} + \dfrac{\beta_4'}{1 + e^{(r-\beta_5')/\beta_6'}} & \text{Air\_Coflow} \end{cases} \tag{6}$$

If $f(r)$ is the temperature profile function, for the flames with N_2 coflow, β_1 and β_2 represent the central and the ambient temperature, respectively; β_3 is the radial position where the temperature is $\frac{\beta_1-\beta_2}{2}$; and β_4 is the gradient of the temperature decline region; for the flames with air co-flow, β_1' and β_4' represent the central flame temperature and the temperature rise near the flame edge,

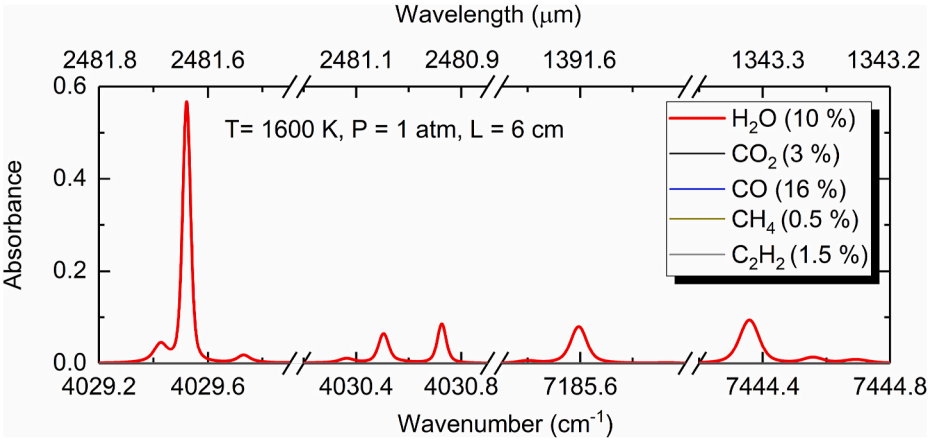

Fig. 1. Spectral simulation of the selected H_2O absorption transitions near 1.4 and 2.5 μm based on HITRAN 2016 database for typical sooting flame conditions: $T = 1600$ K, $P = 1$ atm, $L = 10$ cm, $X_{H2O} = 10\%$, $X_{CO2} = 3\%$, $X_{CO} = 16\%$, $X_{CH4} = 0.5\%$, $X_{C2H2} = 1.5\%$.

respectively; β_2' and β_5' indicate the transition position for temperature decline and rise; β_3' and β_6' are the gradient of the temperature decline region and gradient of the inverse-trapezoid temperature rise region, respectively.

Note that, previous multispectral absorption spectroscopy with profile fitting strategy were mainly used to measure the laminar non-sooting premixed flame with central uniform high-temperature region and monotonic gradient region [28,29,32]. Study on the laminar premixed sooting flame with non-monotonic distribution profiles was sparse. Therefore, the optimal selection of multiple absorption transitions is very important to obtain reliable and accurate measurements. Firstly, the widely-used line selection criteria were utilized for the preliminary screening, mainly including sufficiently strong absorption line-strength and good spectral isolation from interfering species [37,38]. More specifically, for a minimum detectable absorbance of 0.01% and a required SNR over 10 in the atmospheric sooting flame measurements: 800 K $< T <$ 2200 K, $X_{H2O} = 10\%$, $L = 6$ cm, the line-strength should ensure the peak absorbance of >0.1%. For the H_2O absorption-based thermometry, interference from other major combustion products (e.g., CO_2, CO) and intermediates species (CH_4, C_2H_2) should be avoided. Then, the lower state energy (E'') of the selected transitions should be well-separated to ensure good temperature sensitivity in different temperature range [39]. Following the line-selection criteria, we finally select nine absorption transitions near 1.4 and 2.5 μm from the combination and fundamental band within 1–3 μm.

Fig. 1 plots the spectral simulation of the selected absorption transitions under typical sooting flame conditions. All the selected lines have good isolation from other species and sufficient absorbance for detection. The relevant spectroscopic parameters of the selected transitions are listed in Table 1 based on the HITRAN database [40].

3. Experimental details

The target laminar C_2H_4/air premixed sooting flame was stabilized on a standard water-cooled McKenna burner with an inner porous media diameter of 60 mm shielded by an annular co-flow. The flow rates of high purity fuel (99.95%), air (99.99%) and shielding co-flow (99.99%) were precisely and simultaneously monitored by the calibrated mass flow controllers (Sevenstar, ±1% accuracy). Similar to the flame condition in Refs. [9,41], the total flow rate of the fuel mixture was set to be 10 L/min. A series of equivalence ratios ($\Phi = 1.9$, $\Phi = 2.1$, $\Phi = 2.3$) was achieved by varying the C_2H_4 and air flow rates. Table 2 lists the detailed flame conditions. The uncertainty of the overall equivalence ratio was estimated to be within ~ 1.4%. The shielding co-flow of ~10.8 L/min was used to avoid the surrounding air entrainment and fluctuations. Additionally, an extra stainless steel plate was placed 21 mm above the burner to eliminate the flame flickering for better stability. Typical sooting flame images recorded by a digital single lens reflex (SLR) camera was shown in Fig. 2. It is evident to observe the visually yellow radiation from high-temperature soot particles. The blue region around the central flame indicates the outer oxidation due to the co-flow air, which will be quantitatively measured.

A schematic of the optical configuration for sooting flame measurements is illustrated in Fig. 2. Three spectrally-narrow, tunable and continuous-wave distributed feedback (DFB) lasers near 2482 nm (Nanoplus GmbH), 1392 nm (Wuhan Liujiu Inc.) and 1343 nm (Nanjing Qingchen Inc.) were utilized as the single-mode laser sources to target the selected absorption lines. The operation temperature of the DFB lasers was precisely controlled by the commercial low-noise laser drivers (Wavelength Electronics, LDTC 0520) with a standard variation of ~ 0.002 °C during the whole experimental process. The laser injection current was scanned at 2 kHz using triangle waveforms generated by a function generator (TekTronix, AFG3052C) and the signals were sampled at a rate of 4.96 MHz using a multi-channel DAQ card (National Instruments, PCI-6110). Before traveling through the flame, all the collimated laser beams were concentrically aligned using a combination of dichroic mirror and beamsplitter. The transmitted laser beam was separated by a dichroic mirror and focused by convex mirrors onto the photodetectors. To mitigate the significant thermal radiation from the flame, narrow bandpass filters were placed before the photodetectors. In addition to the optical measurements, thermocouple measurement using a fine-wire B-type (Pt–30%Rh vs. Pt–6%Rh) thermocouple (Omega) with a diameter of 0.254 mm was also performed for comparisons. The measured raw thermocouple data were corrected considering the heat-loss correction and reading errors, which were detailed in Refs. [37,42].

Table 1
Spectroscopic parameters of the selected H_2O absorption transitions [40].

Line #	Frequency (cm^{-1})	Wavelength (nm)	S @296 K ($cm^{-2}atm^{-1}$)	E'' (cm^{-1})
1	4029.428	2481.742	9.353×10^{-6}	2748.099
2[a]	4029.524	2481.683	8.497×10^{-5}	2660.944
	4029.524	2481.683	2.834×10^{-5}	2660.945
3	4030.361	2481.167	1.225×10^{-5}	2414.722
4[a]	4030.498	2481.083	5.998×10^{-10}	4902.625
	4030.510	2481.076	1.800×10^{-9}	4902.612
5[a]	4030.728	2480.941	2.146×10^{-9}	4889.485
	4030.729	2480.941	7.153×10^{-10}	4889.486
6[a]	7185.597	1391.673	4.902×10^{-3}	1045.058
	7185.597	1391.673	1.470×10^{-2}	1045.058
7[a]	7444.352	1343.300	5.405×10^{-4}	1774.750
	7444.368	1343.297	1.539×10^{-4}	1806.670
	7444.370	1343.297	4.619×10^{-4}	1806.669
8	7444.563	1343.262	1.555×10^{-4}	1774.615
9	7444.695	1343.238	5.455×10^{-4}	1437.968

[a] Several neighboring transitions with frequency spacing <0.02 cm^{-1} have been considered as one transition.

Table 2
Flame conditions and the corresponding flow rates.

Flame	C_2H_4 (L/min)	Air (L/min)	Co-flow Gas(10.8 L/min)	Φ
1	1.174	8.826	N_2	1.9
2	1.282	8.718	N_2	2.1
3	1.387	8.614	N_2	2.3
4	1.174	8.826	Air	1.9
5	1.282	8.718	Air	2.1
6	1.387	8.614	Air	2.3

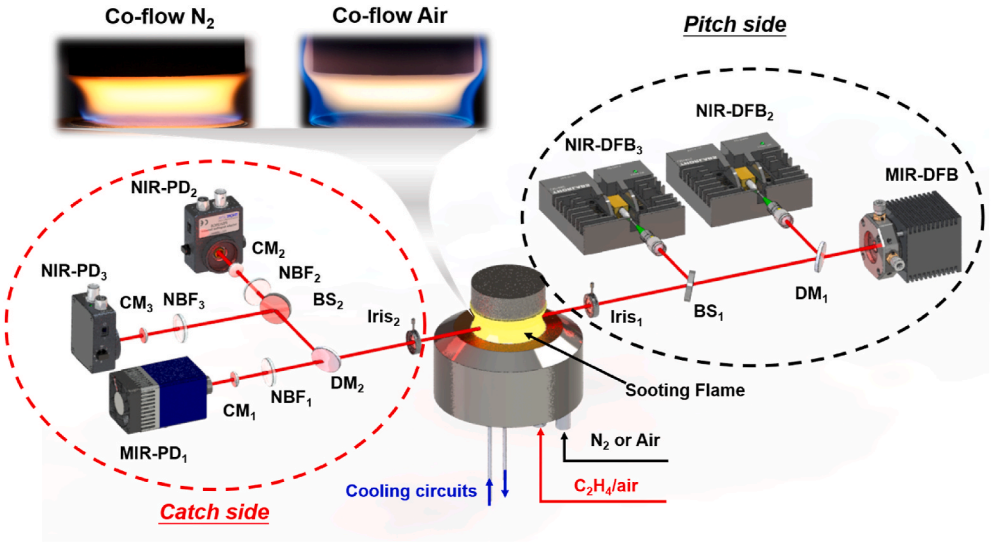

Fig. 2. Schematic of the laser absorption diagnostics in laminar premixed sooting flames. DFB, distributed-feedback diode laser; PD, photodetector; DM, dichroic mirror; BS, beamsplitter; NBF, narrow-band-pass filter; CM, convex mirror.

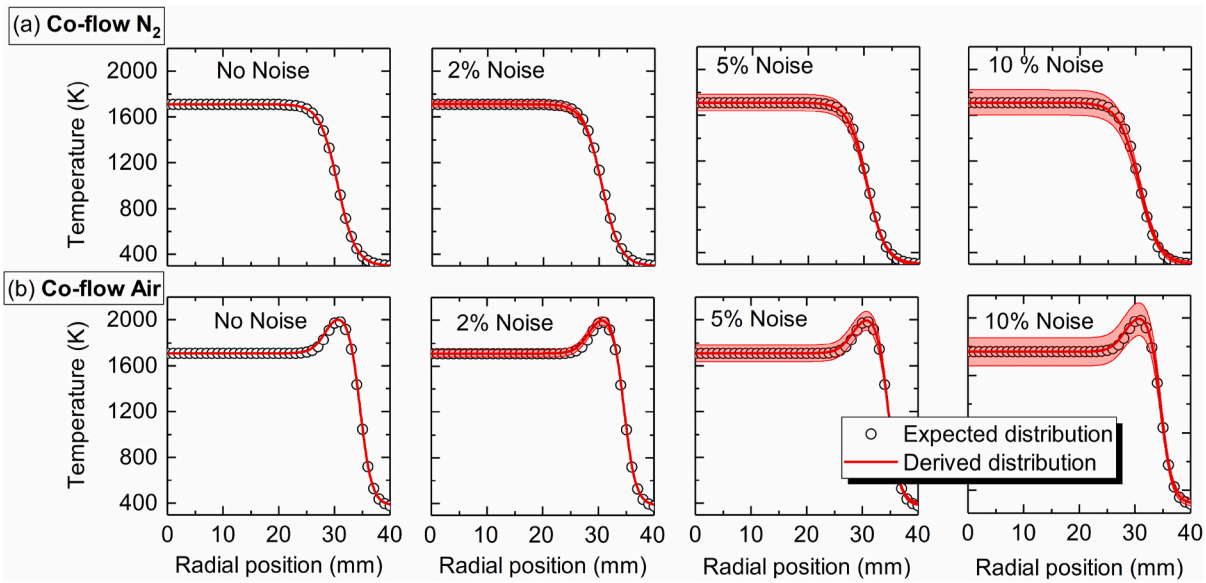

Fig. 3. Simulated radial temperature distributions for sooting flames with (a) nitrogen co-flow and (b) air co-flow under different noise levels. Symbol, the expected distribution; line, the simulated distribution.

4. Results and discussions

4.1. Numerical simulation

We firstly conducted a numerical investigation of the sensor performance for sooting flame temperature measurements. The measurement accuracy and uncertainty are the major factors to be evaluated. Two representative temperature distributions originally obtained from the CARS measurement [9] were selected for the preliminary investigation. One distribution consists of a uniform high-temperature central region and a monotonically decreasing boundary region. The other distribution includes an inverse-trapezoid-like high-temperature region and a monotonically decreasing boundary region. The experimental noise usually influences the accuracy and uncertainty of the final derived results. Therefore, random white noise with a standard deviation of 2–10% was imposed to the integrated absorbance to explore such effects. For each investigated case, simulations were performed 100 times and the mean value of the simulated results was used as the derived results.

The derived temperature distributions under different noise levels (2–10%) are depicted in Fig. 3 with a comparison to the expected distributions. The shaded area indicates the uncertainties mainly from the non-linear least-square fitting and Voigt fitting. For the sooting flames with nitrogen co-flow, as illustrated in Fig. 3(a), the derived temperature agrees well with the expected temperature within ~0.5% in the uniform central high-temperature region. In the boundary region, the derived temperature profiles are in good agreement with the set temperature profiles, but an evident temperature discrepancy exists near the gradient region. The maximum temperature difference is ~50 K, which is below the 10% noise level. For the non-monotonical temperature distribution in sooting flames with air co-flow, the derived temperature distribution agrees well with the expected distribution in the high-temperature region. As illustrated in Fig. 3(b), the relative temperature difference is mostly within ~1% for the noise level below 5% and the maximum relative temperature difference is ~ 2% for the noise level of 10%. The derived temperature profiles within the boundary region also show the evident temperature discrepancies near the gradient region.

In addition to the above two experimentally measured distribution profiles, temperature contours from computational fluid simulations [43] were also selected for performance evaluation. The temperature contours cover a wide temperature range (1500–2200 K). The derived temperature contours and the related absolute temperature difference contours under different noise levels were depicted in Fig. S1 of the supplementary material. For all the cases, the derived results well capture the entire temperature distribution profiles. It is evident that the temperature difference is mostly within 30 K within the high-temperature region. Similar to the findings in Fig. 3, the evident temperature difference lays in the gradient region, mostly within 100 K. Particularly, for the cases with a noise level below 5%, the maximum temperature difference is mostly within ~60 K. Hence, the simulation results indicate that the proposed optical method with high measurement SNR is robust to obtain reliable and appropriate temperature information.

4.2. Experimental results

4.2.1. Raw signal analysis

A comparison of the multi-line and single-line Vogit-fitting was plotted in Fig. 4. For all the spectral features, the multi-line Voigt-fitting gives smaller residuals. In particular, the peak-normalized residuals near the absorption line-center of the multi-line Voigt-

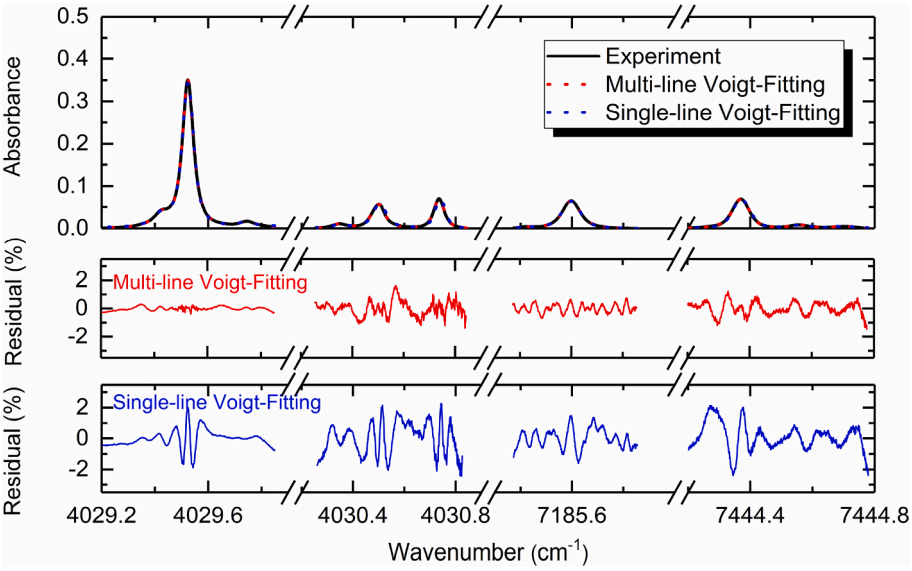

Fig. 4. Representative measurement results with multi-line and single-line best Voigt-fitting profiles. The residuals of the Voigt-fitting are presented at the bottom panels.

fitting are typically 2–10 times smaller than that given by the single-line Voigt-fitting. Therefore, multi-Voigt fitting was used during the Voigt-fitting process.

Typical measurements of raw absorption spectra along with the multi-Voigt fitting profiles for sooting flames with different co-flow gases was depicted in Fig. S2 of the supplementary material. All the absorption features have a high SNR and can be well fitted by the multi-Voigt function. The fractional Voigt-fitting residuals are less than 1.5% over the entire absorption feature for the sooting flames with N_2 coflow and air coflow. The peak absorbance in sooting flames with air coflow is larger than that in sooting flames with N_2 Co-flow, which is due to the higher temperature and gas concentrations within the region where the unburnt fuel, intermediate products (e.g., CH_4, C_2H_2 and H_2) and generated soot re-burns with the coflow air. In particular, the residuals near the line-center of the selection absorption lines are typically below 0.5%. Such a small fitting residual indicates the appropriate spectral fitting process and accurate integrated area of the absorbance, which ensures reliable and appropriate measurement results. The fitting residuals and non-linear least-square fitting error are mainly considered to estimate the measurement uncertainties.

4.2.2. Discussion

Firstly, we select the ISF target sooting flame at $\Phi = 2.1$ for experimental demonstrations. The measured radial temperature distributions are depicted in Fig. 5 and are compared with the CARS measurements [9]. The LAS-determined temperature profiles are observed to be almost identical to the CARS and thermocouple measurements. More specifically, in the central uniform region, the LAS measurement agrees well with the CARS and thermocouple measurements within 7.7% and 1.4%, respectively. The LAS measurement also well captures the decline transition position in the boundary region and the raise transition position in the inverse-trapezoid-like region. Similar to the findings in Section 4.1, the measurement discrepancies mainly lay around the gradient region. The thermocouple-determined temperature agrees well with the CARS measurement mostly within 80 K, which indicates it can be a good reference for comparisons.

Fig. 6 depicts the measured axial distribution of flame temperature along height above the burner (HAB). The LAS results at different equivalence ratios are compared with the thermocouple measurements to show the good agreements, mostly within a relative difference of ~42 K. The maximum temperature difference between the LAS and thermocouple measurements occurs at HAB = 13 mm with $\Phi = 2.3$. Additionally, temperature results obtained by the LAS-based two-line thermometry and thermocouple measurements from the literature [41] are also plotted in Fig. 6 for comparison, showing a relatively good agreement. The temperature measured by multi-spectral LAS is consistently higher than the results obtained by the LAS-based two-line thermometry. This is because the cool thermal boundary layer near the flame edge reduced the derived temperature. The evident temperature decrease at HAB = 5–15 mm is due to the strong heat radiative loss of high-temperature gas products and soot particles, as well as the heat sink effect of the stabilized plate. The highest temperature is within a HAB of 3–5 mm, where strong fuel oxidation occurs.

Fig. 7 presents the measured radial distribution of temperature at three representative HAB positions, including scarce sooting positions (HAB = 3 mm), slight sooting positions (HAB = 9 mm), and significant sooting positions (HAB = 15 mm). For each HAB, the LAS measured temperature agrees reasonably well with the thermocouple measurement, particularly in the central high-temperature region. For flames with N_2 co-flow, the radial temperature remains almost constant in the central region and then decreases to the ambient condition. However, for the flames with air co-flow, the radial temperature remains almost stable till the edge of the fuel-mixture stream, and then experiences an increase before falling to the ambient condition. For a fixed equivalence ratio and HAB, the central temperature was observed to have a slight increase (10–24 K) when the co-flow was switched from N_2 to air. Such a slight temperature increase is due to the enhanced flame heat transfer from the re-ignition high-temperature region near the flame edge. The re-ignition is mainly due to the oxidation of the combustible products by oxygen in the air co-flow. At the same HAB, the radius of the central uniform region for flames with different co-flow gases is almost identical. For the flames with air co-flow, the radial position of

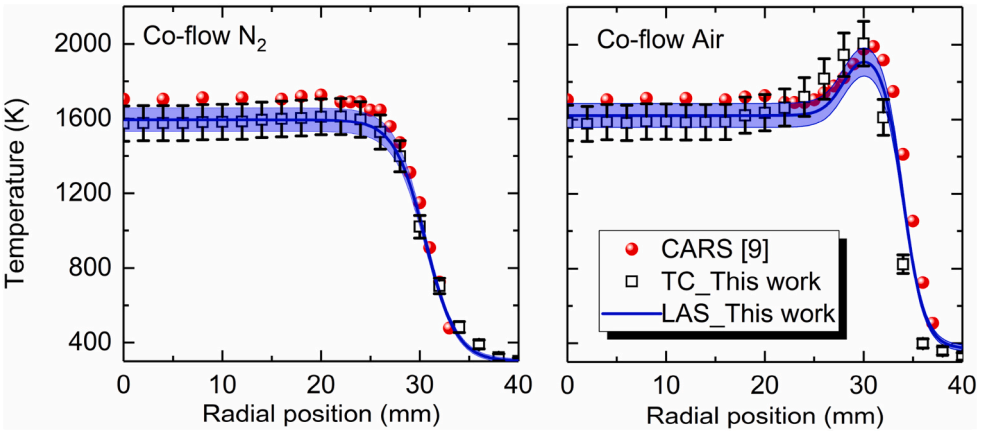

Fig. 5. Comparison of the radial temperature distribution for sooting flames at $\Phi = 2.1$ under different co-flow conditions. Blue line: LAS measurement; Black symbol: thermocouple (TC) measurement; Red symbol: CARS measurement [9]. (For interpretation of the references to colour in this figure legend, the reader is referred to the Web version of this article.)

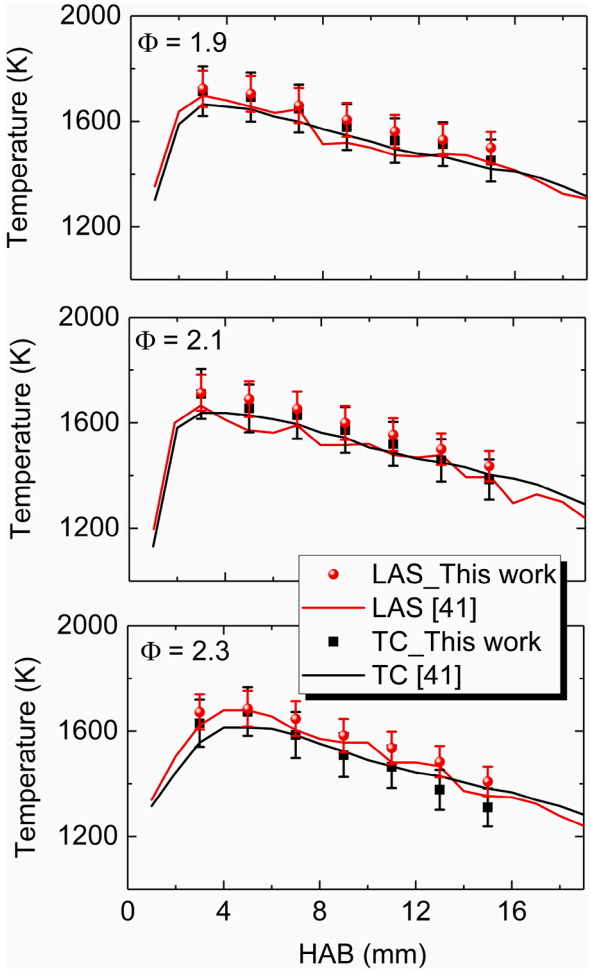

Fig. 6. Measured central flame temperature along the HAB in sooting flames at different equivalence ratio (Φ = 1.9, 2.1 and 2.3).

the highest temperature locates near the boundary where the reactants interact with the co-flow.

Fig. 8 summarizes the radial temperature distribution at different HABs in a contour plot to visualize the thermal structures of the sooting flames. The LAS measurements are compared with the thermocouple data at different equivalence ratios and co-flows. The spatial resolution of the LAS-measured contour along the HAB and radial direction are 2 mm and 1 mm, respectively. For each case, the LAS and thermocouple measurements provided almost identical radial and axial distribution profiles of temperature. More specifically, the LAS measurement well captures the central uniform high-temperature region with a radius of ~25 mm for the flames with nitrogen co-flow and the inverse-trapezoid-like high-temperature region with a radius of ~32 mm for the flames with air co-flow.

For the case study in axisymmetric laminar premixed sooting flames, the developed measurement technique is demonstrated to be reliable and appropriate to provide accurate temperature results. Note that, the application of current measurement technique in turbulent flames or unsymmetrical laminar flames is quite challenging. For unsymmetric laminar flames, it can be solved probably by adopting the tomography reconstruction method to obtain the basic distribution profiles of the flame, and then information of the similar flames can be measured using the line-of-sight absorption with presumed profile. For turbulent flames, by considering the effect of turbulence and using high-bandwidth (kHz-MHz) modulation strategy, time-averaged and time-resolved profiles of the turbulent reaction zone can be obtained.

5. Conclusions

In this work, we demonstrated the multispectral infrared thermometry for quantitative measurements of temperature field in sooting flames with different co-flow conditions using three tunable DFB lasers. Multiple H_2O absorption transitions within the combination and fundamental ro-vibrational band ($\nu_1+\nu_3$, ν_3) were probed for accurate and sensitive temperature measurements using scanned-wavelength DAS. The technique was firstly validated against the data provided in the literature under the same flame condition. Good agreement was found between the measured results and the literature data in terms of the axial and radial distributions of temperature. The optical measurements were then compared with the thermocouple measurements to show the successfully captured

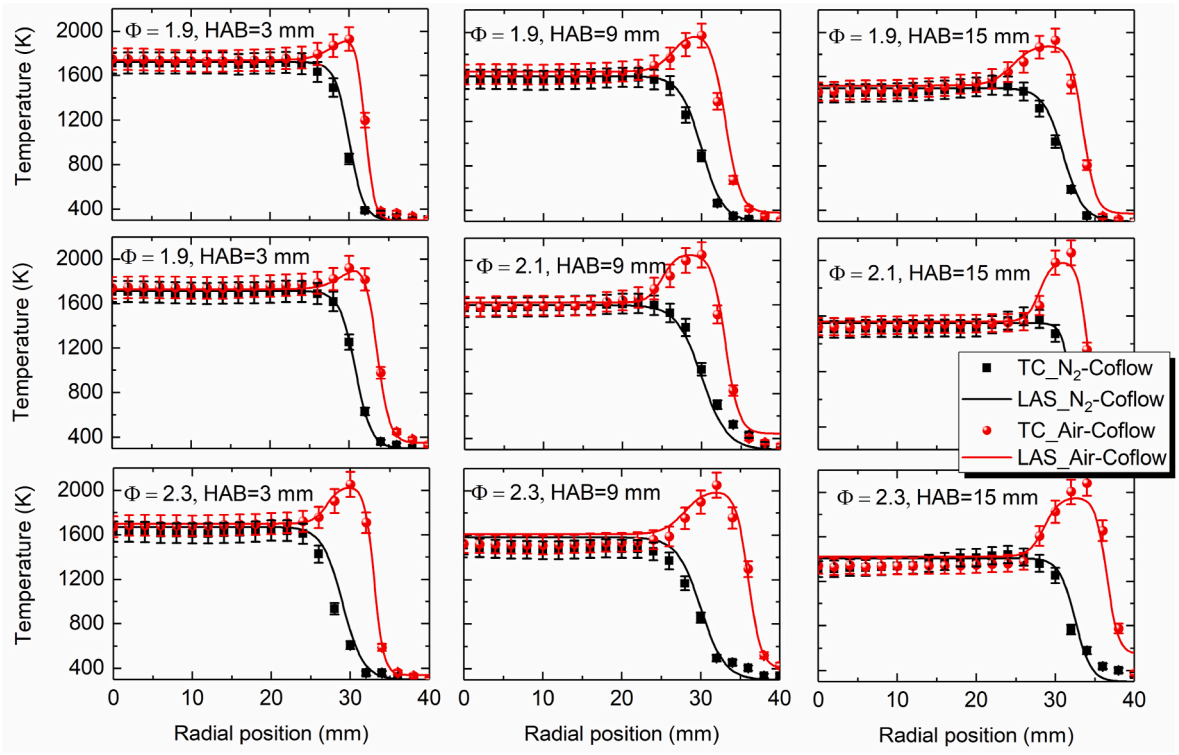

Fig. 7. Measured central flame temperature along the HAB in sooting flames with N_2 co-flow at different equivalence ratios (Φ = 1.9, 2.1 and 2.3).

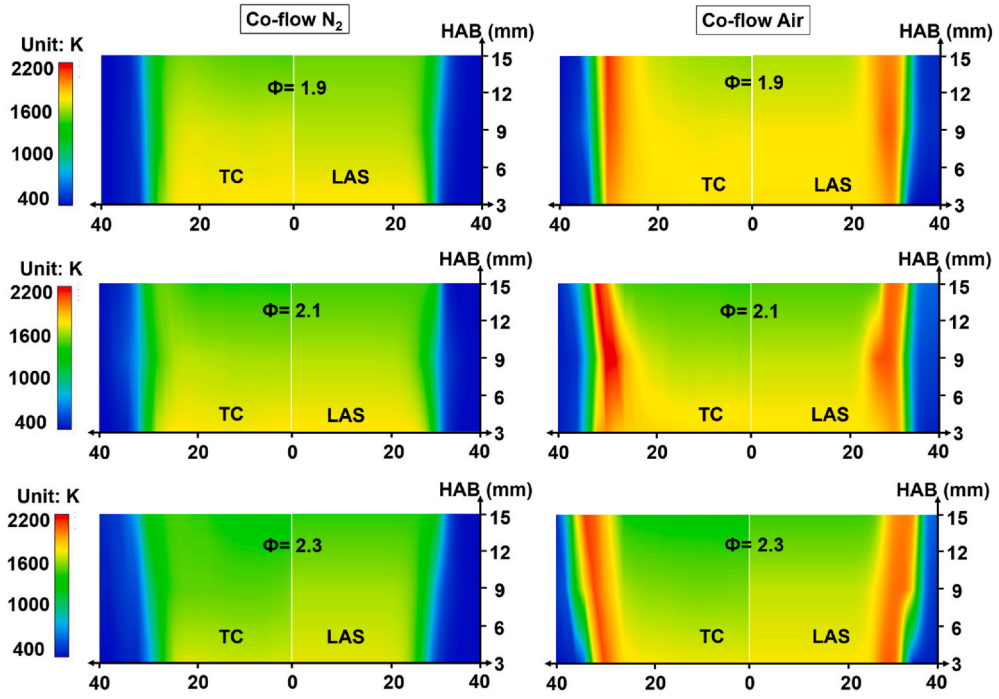

Fig. 8. Temperature contours for C_2H_4/air sooting flames at different equivalence ratios and various co-flow gas types. The LAS measurements are compared with the thermocouple data.

temperature field. The slight temperature difference between different co-flow conditions reflects the enhanced heat transfer from the re-ignition high-temperature region near the flame edge. The successful differentiation of such a nuance indicates the superior sensitivity of the current method. The method described in the present work shows good potential for sensitive temperature sensing in sooting flames. To the best of our knowledge, this is the first quantitative measurement of temperature distributions in the laminar premixed sooting flame using multispectral infrared absorption spectroscopy. If the tomography reconstruction method and high-bandwidth (kHz-MHz) modulation strategy are adopted, the spatiotemporal resolution of the current method can be improved and has the potential of being used in combustion diagnostics of highly-transient or unsymmetrical flames.

Author statement

Liuhao Ma: Conceptualization, Methodology, Investigation, Formal analysis, Visualization, Writing - original draft. Kun Duan: Investigation, Formal analysis, Writing - review & editing. Kin-Pang Cheong: Formal analysis, Visualization, Writing - review & editing. Chaokai Yuan: Investigation, Writing - review & editing. Wei Ren: Conceptualization, Investigation, Writing - review & editing, Supervision.

Declaration of competing interest

The authors declare that they have no known competing financial interests or personal relationships that could have appeared to influence the work reported in this paper.

Acknowledgements

This research is supported by National Natural Science Foundation of China (NSFC) (52106221, 52006152, 51776179), Open Funding from State Key Laboratory of High-temperature Gas Dynamics, and Fundamental Research Funds for the Central Universities (WUT:2021IVA016) and Startup funding of Wuhan University of Technology (40120607). Prof. Kin-Pang Cheong also acknowledges the support from Science Foundation of Sichuan Province (No. 2020JDRC0034) and the Fundamental Research Funds for the Central Universities (No. YJ202019).

Appendix A. Supplementary data

Supplementary data to this article can be found online at https://doi.org/10.1016/j.csite.2021.101575.

References

[1] H. Wang, Formation of nascent soot and other condensed-phase materials in flames, Proc. Combust. Inst. 33 (1) (2011) 41–67.
[2] F.N. Egolfopoulos, N. Hansen, Y. Ju, K. Kohse-Höinghaus, C.K. Law, F. Qi, Advances and challenges in laminar flame experiments and implications for combustion chemistry, Prog. Energy Combust. Sci. 43 (2014) 36–67.
[3] N.-E. Olofsson. Laser-induced Incandescence and Complementary Diagnostics for Flame Soot Characterization, Lund University, 2014.
[4] J. Appel, H. Bockhorn, M. Frenklach, Kinetic modeling of soot formation with detailed chemistry and physics: laminar premixed flames of C2 hydrocarbons, Combust. Flame 121 (1–2) (2000) 122–136.
[5] J. Camacho, C. Liu, C. Gu, H. Lin, Z. Huang, Q. Tang, et al., Mobility size and mass of nascent soot particles in a benchmark premixed ethylene flame, Combust. Flame 162 (10) (2015) 3810–3822.
[6] Y. Zhang, Y. Li, P. Liu, R. Zhan, Z. Huang, H. Lin, Investigation on the chemical effects of dimethyl ether and ethanol additions on PAH formation in laminar premixed ethylene flames, Fuel 256 (2019), 115809.
[7] International Sooting Flame (ISF), Workshop available at: https://www.adelaide.edu.au/cet/isfworkshop/. 2012.
[8] F. Migliorini, S. De Iuliis, F. Cignoli, G. Zizak, How "flat" is the rich premixed flame produced by your McKenna burner? Combust. Flame 153 (3) (2008) 384–393.
[9] N.-E. Olofsson, H. Bladh, A. Bohlin, J. Johnsson, P.-E. Bengtsson, Are sooting premixed porous-plug burner flames one-dimensional? A laser-based experimental investigation, Combust. Sci. Technol. 185 (2) (2013) 293–309.
[10] W. Pejpichestakul, A. Cuoci, A. Frassoldati, M. Pelucchi, A. Parente, T. Faravelli, Buoyancy effect in sooting laminar premixed ethylene flame, Combust. Flame 205 (2019) 135–146.
[11] Y. Xuan, G. Blanquart, Two-dimensional flow effects on soot formation in laminar premixed flames, Combust. Flame 166 (2016) 113–124.
[12] H. Böhm, D. Hesse, H. Jander, B. Lüers, J. Pietscher, H. Wagner, et al., The influence of pressure and temperature on soot formation in premixed flames, Symposium (International) on combustion 22 (1989) 403–411. Elsevier.
[13] D. Olson, S. Madronich, The effect of temperature on soot formation in premixed flames, Combust. Flame 60 (2) (1985) 203–213.
[14] W. Wang, L. Xu, J. Yan, Y. Wang, Temperature dependence of the fuel mixing effect on soot precursor formation in ethylene-based diffusion flames, Fuel 267 (2020), 117121.
[15] N.J. Kempema, R.R. Dobbins, M.B. Long, M.D. Smooke, Constrained-temperature solutions of coflow laminar diffusion flames, Proc. Combust. Inst. 38 (2021) 1905–1912.
[16] C.R. Shaddix. Correcting Thermocouple Measurements for Radiation Loss: A Critical Review, Sandia National Labs., Livermore, CA (US), 1999.
[17] H. Liu, S. Zheng, H. Zhou, Measurement of soot temperature and volume fraction of axisymmetric ethylene laminar flames using hyperspectral tomography, IEEE Transactions on Instrumentation and Measurement 66 (2) (2016) 315–324.
[18] J. Sun, M.M. Hossain, C. Xu, B. Zhang, Investigation of flame radiation sampling and temperature measurement through light field camera, Int. J. Heat Mass Tran. 121 (2018) 1281–1296.
[19] S.P. Kearney, M.N. Jackson, Dual-pump coherent anti-Stokes Raman scattering thermometry in heavily sooting flames, AIAA J. 45 (12) (2007) 2947–2956.

[20] B. Zhou, C. Brackmann, Q. Li, Z. Wang, P. Petersson, Z. Li, et al., Distributed reactions in highly turbulent premixed methane/air flames: Part I. Flame structure characterization, Combust. Flame 162 (7) (2015) 2937–2953.
[21] J.J. Girard, R.M. Spearrin, C.S. Goldenstein, R.K. Hanson, Compact optical probe for flame temperature and carbon dioxide using interband cascade laser absorption near 4.2 μm, Combust. Flame 178 (2017) 158–167.
[22] R.K. Hanson, D.F. Davidson, Recent advances in laser absorption and shock tube methods for studies of combustion chemistry, Prog. Energy Combust. Sci. 44 (2014) 103–114.
[23] C.S. Goldenstein, R.M. Spearrin, J.B. Jeffries, R.K. Hanson, Infrared laser-absorption sensing for combustion gases, Prog. Energy Combust. Sci. 60 (2017) 132–176.
[24] C. Liu, L. Xu, Laser absorption spectroscopy for combustion diagnosis in reactive flows: a review, Appl. Spectrosc. Rev. 54 (1) (2019) 1–44.
[25] X. Liu, J.B. Jeffries, R.K. Hanson, Measurement of non-uniform temperature distributions using line-of-sight absorption spectroscopy, AIAA J. 45 (2) (2007) 411–419.
[26] K.-P. Cheong, L. Ma, Z. Wang, W. Ren, Influence of line pair selection on flame tomography using infrared absorption spectroscopy, Appl. Spectrosc. 73 (5) (2019) 529–539.
[27] P. Nau, J. Koppmann, A. Lackner, K. Kohse-Höinghaus, A. Brockhinke, Quantum cascade laser-based MIR spectrometer for the determination of CO and CO_2 concentrations and temperature in flames, Appl. Phys. B 118 (3) (2015) 361–368.
[28] G. Zhang, J. Liu, Z. Xu, Y. He, R. Kan, Characterization of temperature non-uniformity over a premixed CH_4–air flame based on line-of-sight TDLAS, Appl. Phys. B 122 (1) (2016) 3.
[29] L.H. Ma, L.Y. Lau, W. Ren, Non-uniform temperature and species concentration measurements in a laminar flame using multi-band infrared absorption spectroscopy, Appl. Phys. B 123 (3) (2017) 83.
[30] X. Liu, G. Zhang, Y. Huang, Y. Wang, F. Qi, Two-dimensional temperature and carbon dioxide concentration profiles in atmospheric laminar diffusion flames measured by mid-infrared direct absorption spectroscopy at 4.2 μm, Appl. Phys. B 124 (4) (2018) 61.
[31] C. Wei, D.I. Pineda, L. Paxton, F.N. Egolfopoulos, R.M. Spearrin, Mid-infrared laser absorption tomography for quantitative 2D thermochemistry measurements in premixed jet flames, Appl. Phys. B 124 (6) (2018) 123.
[32] L. Ma, K.-P. Cheong, H. Ning, W. Ren, An improved study of the uniformity of laminar premixed flames using laser absorption spectroscopy and CFD simulation, Exp. Therm. Fluid Sci. 112 (2020), 110013.
[33] Z. Wang, Y. Deguchi, T. Kamimoto, K. Tainaka, K. Tanno, Pulverized coal combustion application of laser-based temperature sensing system using computed tomography–Tunable diode laser absorption spectroscopy (CT-TDLAS), Fuel 268 (2020), 117370.
[34] C. Liu, Z. Cao, F. Li, Y. Lin, L. Xu, Flame monitoring of a model swirl injector using 1D tunable diode laser absorption spectroscopy tomography, Meas. Sci. Technol. 28 (5) (2017), 054002.
[35] C. Wei, D.I. Pineda, C.S. Goldenstein, R.M. Spearrin, Tomographic laser absorption imaging of combustion species and temperature in the mid-wave infrared, Opt Express 26 (16) (2018) 20944–20951.
[36] R.K. Hanson, R.M. Spearrin, C.S. Goldenstein, Spectroscopy and Optical Diagnostics for Gases, Springer, 2016.
[37] L. Ma, H. Ning, J. Wu, W. Ren, In situ flame temperature measurements using a mid-Infrared two-line H_2O laser-absorption thermometry, Combust. Sci. Technol. 190 (3) (2018) 393–408.
[38] C.S. Goldenstein, I.A. Schultz, J.B. Jeffries, R.K. Hanson, Two-color absorption spectroscopy strategy for measuring the column density and path average temperature of the absorbing species in nonuniform gases, Appl. Opt. 52 (33) (2013) 7950–7962.
[39] X. Liu, Line-of-sight Absorption of H_2O Vapor Gas Temperature Sensing in Uniform and Nonuniform Flows, Stanford University Stanford, CA, 2006.
[40] I. Gordon, L. Rothman, C. Hill, R. Kochanov, Y. Tan, P. Bernath, et al., The HITRAN2016 molecular spectroscopic database, J. Quant. Spectrosc. Radiat. Transf. 203 (2017) 3–69.
[41] Q. Wu, F. Wang, M. Li, J. Yan, K. Cen, Simultaneous in-situ measurement of soot volume fraction, H_2O concentration, and temperature in an ethylene/air premixed flame using tunable diode laser absorption spectroscopy, Combust. Sci. Technol. 189 (9) (2017) 1571–1590.
[42] C.S. McEnally, Ü.Ö. Köylü, L.D. Pfefferle, D.E. Rosner, Soot volume fraction and temperature measurements in laminar nonpremixed flames using thermocouples, Combust. Flame 109 (4) (1997) 701–720.
[43] L. Ma, H. Ning, J. Wu, K.-P. Cheong, W. Ren, Characterization of temperature and soot volume fraction in laminar premixed flames: laser absorption/extinction measurement and two-dimensional computational fluid dynamics modeling, Energy Fuel. 32 (12) (2018) 12962–12970.